

# Neutrino masses from clustering of red and blue galaxies: a test of astrophysical uncertainties

Molly E. C. Swanson,<sup>1,2\*</sup> Will J. Percival,<sup>3</sup> and Ofer Lahav<sup>1</sup>

<sup>1</sup>*Department of Physics and Astronomy, University College London, Gower Street, London, WC1E 6BT, UK*

<sup>2</sup>*Harvard-Smithsonian Center for Astrophysics, 60 Garden Street, Cambridge, MA 02138, USA*

<sup>3</sup>*Institute of Cosmology and Gravitation, University of Portsmouth, Dennis Sciama building, Portsmouth, P01 3FX, UK*

8 June 2018

## ABSTRACT

Combining measurements of the galaxy power spectrum and the cosmic microwave background (CMB) is a powerful means of constraining the summed mass of neutrino species  $\sum m_\nu$ , but is subject to systematic uncertainties due to non-linear structure formation, redshift-space distortions and galaxy bias. We empirically test the robustness of neutrino mass results to these effects by separately analyzing power spectra of red and blue galaxies from the Sloan Digital Sky Survey (SDSS-II) Data Release 7 (DR7), combined with the CMB five-year Wilkinson Microwave Anisotropy Probe (WMAP5) data. We consider fitting for a range of maximum wavenumber  $k$  using twelve different galaxy bias models. For example, using a new model based on perturbation theory and including redshift space distortions (Saito et al. 2009), the all-galaxy power spectrum combined with WMAP5 for a wavenumber range of  $k < 0.2 h \text{ Mpc}^{-1}$  yields 95% CL  $\sum m_\nu < 0.46 \text{ eV}$ . The red and blue galaxy power spectra give 0.41 and 0.63 eV respectively for this model. Using mock catalogues, we find the expected difference in these limits assuming a true neutrino mass of zero is  $0.10 \pm 0.14 \text{ eV}$ . Thus the difference of 0.22 eV between upper limits on neutrino mass for red and blue galaxies is approximately  $1\sigma$  from the expected value. We find similar results for the other models and  $k$  ranges tested. This indicates good agreement for current data but hints at possible issues for next-generation surveys. Being able to perform such systematic tests is advantageous, and future surveys would benefit by including broad galaxy populations and luminosities that enable such a decomposition.

**Key words:** neutrinos – cosmological parameters – cosmology: observations – galaxies: statistics – cosmic background radiation – large-scale structure of Universe.

## 1 INTRODUCTION

Atmospheric and solar neutrino experiments show that neutrinos have mass and that there is significant mixing between the various neutrino interaction eigenstates (Davis 1996; Fukuda et al. 1998; Ahmad et al. 2002; Ashie et al. 2005; Martin 2009; Wendell et al. 2010). Cosmological measurements nicely complement these experiments by constraining the sum of the masses of the different eigenstates  $\sum_i m_{\nu_i}$ . The cosmological experiments exploit differences between the behaviour of cold dark matter (CDM) and massive neutrinos, which free-stream when relativistic, removing small-scale structure that would have formed in a CDM-only universe (for recent reviews see, e.g., Elgarøy & Lahav 2005; Lesgourgues & Pastor 2006; Hannestad 2010). To first order, the suppression depends on  $\Omega_\nu$ , the total mass density

comprised of neutrinos relative to the critical density of the Universe. This is related to the sum of the mass eigenstates by  $\sum m_\nu = \Omega_\nu (94.1 h^2 \text{ eV})$ , where  $h$  is the Hubble constant  $H_0$  divided by  $100 \text{ km s}^{-1} \text{ Mpc}^{-1}$ . Thus cosmological measurements primarily probe the total particle mass summed over neutrino species. In principle, the neutrino mass hierarchy could be measured by resolving the free-streaming scale of individual neutrino species, but current experiments do not have the sensitivity required to do this (Hannestad 2003; Takada et al. 2006; Jimenez et al. 2010).

The most recent upper limit on the summed neutrino mass published by the Wilkinson Microwave Anisotropy Probe (WMAP) team is  $\sum m_\nu < 0.58 \text{ eV}$  at 95% CL (Komatsu et al. 2010). This limit combines CMB data from the 7 year WMAP data release (WMAP7) with a measurement of  $H_0$  from type Ia supernovae (SN Ia) and the Baryon Acoustic Oscillation (BAO) information from the 2-degree Field Galaxy Redshift Survey (2dFGRS) and Sloan Digital

\* E-mail: molly@star.ucl.ac.uk

Sky Survey (SDSS-II). Adding large scale structure information from surveys of galaxies, galaxy clusters, or weak lensing pushes this limit down even further: other groups have combined WMAP5 with SN Ia, BAO, and large scale structure information and derive limits as low as  $\sum m_\nu < 0.28$  eV at 95% CL (e.g., Vikhlinin et al. 2009; Tereno et al. 2009; Reid et al. 2010a; Mantz et al. 2010; Thomas et al. 2010). The challenge now is to reliably bring down the upper limits to the 0.1 eV level or even detect the neutrino mass using the next generation of galaxy survey and CMB data (Lesgourgues et al. 2004; Lesgourgues & Pastor 2006; Hannestad & Wong 2007; Lahav et al. 2010).

Unfortunately, our ability to measure the summed neutrino mass using large scale structure information such as the galaxy power spectrum will likely be limited by our lack of knowledge about other effects that change the expected amplitude of galaxy clustering on small-scales. These effects include the formation of non-linear matter structures and the non-linear galaxy peculiar velocities within these structures. The peculiar velocities affect the measured power spectrum because we infer distances from redshifts, and peculiar velocities are misinterpreted as being due to the Hubble flow. Thus the random motion of galaxies within collapsed structures acts to damp the power spectrum on small scales.

In addition, galaxies are not expected to exactly Poisson sample the distribution of matter in the Universe (Sheth & Lemson 1999; Casas-Miranda et al. 2002); evidence for this has been seen in, e.g., Wake et al. (2008). This severely complicates the extraction of cosmological information from galaxy surveys. Furthermore, it has been known for some time that different populations of galaxies demonstrate different clustering strengths (Davis & Geller 1976; Dressler 1980; Park et al. 1994; Peacock & Dodds 1994; Seaborne et al. 1999; Norberg et al. 2001, 2002; Zehavi et al. 2002, 2005; Wild et al. 2005; Collister & Lahav 2005; Li et al. 2006; Swanson et al. 2008), showing that they cannot all have a simple relationship linking their distribution with that of the matter. This galaxy bias (the relationship between the galaxies and the matter) is the most pernicious physical effect that limits our ability to extract cosmological data from galaxy surveys (Percival et al. 2007; Sánchez & Cole 2008).

Because of the uncertainty regarding these effects, many cosmologists (including the WMAP team) choose not to use the galaxy power spectrum in making their cosmological parameter constraints (Dunkley et al. 2009; Komatsu et al. 2010) and instead encapsulate the information from galaxy surveys as a prior on the geometrical distance to the mean redshift of the galaxy survey based on using the BAO acoustic peak as a standard ruler. This is effective but discards a great deal of information contained in the shape of the power spectrum that is especially valuable for making neutrino mass constraints. In order to fully exploit the information contained in the galaxy distribution, we must develop a more sophisticated understanding of how the power spectrum is affected by galaxy bias, non-linear evolution, and redshift space distortions. Of these three systematic effects, the galaxy bias is in some sense the most troublesome: non-linear evolution and redshift space distortions can be studied in N-body simulations allowing only for evolution through gravity, but modelling galaxy bias in detail requires hydro-

dynamic simulations or semi-analytic galaxy formation models.

The aim of this paper is to quantify the impact of these systematic effects on measurements of the summed neutrino mass from the galaxy power spectrum, focusing especially on the effects of galaxy bias. We use data from the final data release of the SDSS-II survey, which we split into the bimodal populations of blue and red galaxies. By comparing results from two galaxy populations with differing properties, we can study the impact of astrophysical effects while bypassing the need to model biasing in detail. We also consider how the range of wavenumber  $k$  fitted affects the results. Using data at larger  $k$  values adds more information about neutrinos from the effects on the small-scale structure, but it comes at the price of requiring more complicated theoretical modelling. We fit our subsamples and the combined sample with 12 different power spectrum models and combine with CMB constraints from WMAP5.

This work is timely for two reasons. Firstly, the upcoming generation of galaxy surveys such as the Dark Energy Survey (DES; Abbott et al. 2006), the Panoramic Survey Telescope & Rapid Response System (Pan-STARRS; Morgan & Kaiser 2008; Morgan et al. 2008), and the Large Synoptic Survey Telescope (LSST; Abell et al. 2009) will significantly reduce the statistical uncertainty on power spectrum measurements, making a detailed understanding of the systematic uncertainties increasingly essential. Secondly, we can now make use of new perturbation theory results that provide more accurate models for the non-linear matter power spectrum including neutrinos (Saito et al. 2009; Taruya et al. 2009): along with Saito et al. (2010) this analysis is one of the first applications of these models to observational data.

This paper is organised as follows. We start by describing the data that we use in Section 2. The method by which these data are analysed, including power spectrum calculation and likelihood analysis is described in Section 3. Results are presented in Section 4, and are discussed in Section 5. For simplicity, here we assume a cosmological model of flat  $\Lambda$ CDM plus massive neutrinos, but we note that alternative cosmological models (in particular those with dark energy equation of state  $w \neq -1$ ) can impact neutrino mass measurements as well (Hannestad 2005; Kiakotou et al. 2008; Reid et al. 2010a) and will be investigated further in future work. Specifically, we fix  $\Omega_M + \Omega_\Lambda = 1$ , the dark energy equation of state  $w = -1$ , the tensor amplitude and running of the spectral index to zero, and the effective number of relativistic degrees of freedom  $N_{\text{eff}} = 3.04$ . We convert galaxy redshifts to distances using  $\Omega_M = 0.25$  and  $\Omega_\Lambda = 0.75$ , and assume that this is the true cosmology when estimating errors on these measurements.

## 2 DATA

### 2.1 Galaxy data

The SDSS-II experiment used a 2.5m telescope (Gunn et al. 2006), to obtain a spectroscopic sample of galaxies selected to a limiting Galactic extinction-corrected Petrosian magnitude  $r < 17.77$ , or  $r < 17.5$  in a small subset of the early data from the survey (Strauss et al. 2002). There are

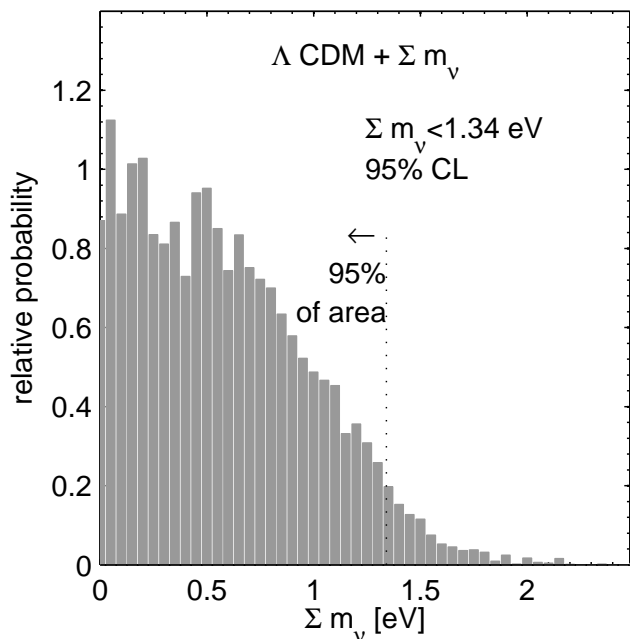


**Figure 1.** Histogram of the probability distribution for  $\sum m_\nu$  reproduced using the WMAP5 MCMC chain from Dunkley et al. (2009).

approximately 90 galaxies per square degree, with a median redshift of  $z = 0.1$ . The DR7 sample (Abazajian et al. 2009) used in our analysis includes 669 905 main galaxies (Strauss et al. 2002). We correct for fibre packing problems where close galaxies cannot both be observed by assigning the redshift of the nearest observed galaxy to a galaxy which was not observed, matching the methodology of Zehavi et al. (2002). This is the subsample of SDSS main galaxies used by Percival et al. (2010). Galaxy redshifts were converted to distances using our fiducial cosmology (flat  $\Lambda$ CDM model with  $\Omega_m = 0.25$ ).

We have  $k$ -corrected galaxy luminosities using the methodology outlined in Blanton et al. (2003a,b). We also use a  $z = 0.1$  shifted  $r$ -band filter to define our luminosities (as discussed in Blanton et al. 2003a,b), which we refer to as  $M_{0.1,r}$ . Absolute magnitudes and  $k$ -corrections were calculated assuming  $H_0 = 100 \text{ km s}^{-1} \text{ Mpc}^{-1}$ , and our fiducial cosmology, and we have applied the recommended AB corrections to the observed SDSS magnitude system (Smith et al. 2002).

This sample of galaxies was split into red and blue subsamples defined by a constant colour cut of  $M_{0.1,g} - M_{0.1,r} = 0.8$ . This approximately divides the bimodal distribution of galaxies into red and blue types (e.g. Cresswell & Percival 2009). Our results are not sensitive to the exact nature of this division. The red and blue subsamples have median redshifts of  $z = 0.111$  and  $z = 0.085$  respectively.

## 2.2 CMB data

We use the WMAP5 CMB data as our baseline for neutrino mass constraints (Dunkley et al. 2009). The WMAP5 CMB data alone provide a limit of  $\sum m_\nu < 1.3 \text{ eV}$  (95% CL), robust to within 10% to varying tensor amplitude, run-

ning spectral index, or dark energy equation of state  $w$ . As discussed in Ichikawa et al. (2005), the best one can hope to do for the neutrino mass limit using only CMB data is  $\sum m_\nu \lesssim 1.2 \text{ eV}$ . Since the WMAP5 limit is already nearly at this value, we do not expect significant improvement by going to WMAP7. This is borne out by the fact that the WMAP7-only limit is also  $\sum m_\nu < 1.3 \text{ eV}$  (Komatsu et al. 2010).

We have downloaded the WMAP5  $\Lambda$ CDM+ $M_\nu$  MCMC chain from Dunkley et al. (2009) from the LAMBDA archive<sup>1</sup>. This model uses eight parameters to fit to the CMB temperature and polarization power spectra: the cold dark matter density  $\Omega_c h^2$ , the baryon density  $\Omega_b h^2$ , the neutrino mass density  $\Omega_\nu h^2$ , the dark energy density  $\Omega_\Lambda$ , the amplitude of curvature fluctuations  $\Delta_{\mathcal{R}}^2$ , the scalar spectral index  $n_s$ , the reionization optical depth  $\tau$ , and the amplitude  $A_{\text{SZ}}$  of a Sunyaev-Zel'dovich (SZ, Sunyaev & Zeldovich 1970) fluctuation template spectrum. We express these parameters in a more digestible form using the flatness assumption,  $\sum m_\nu = \Omega_\nu (94.1 h^2 \text{ eV})$ , and the definition of the linear theory density fluctuation amplitude at  $8 h^{-1} \text{ Mpc}$  scales:

$$\sigma_8 \equiv \left\{ \frac{1}{2\pi^2} \int_0^\infty [3(\sin x - x \cos x)/x^3]^2 P_{\text{lin}}(k) k^2 dk \right\}^{1/2} \quad (1)$$

with  $x \equiv k \times 8 h^{-1} \text{ Mpc}$ . This gives a parameter set  $\theta^i \equiv (\Omega_\Lambda, \Omega_b/\Omega_m, h, \sigma_8, n_s, \sum m_\nu)$  plus the CMB-only parameters ( $\tau, A_{\text{SZ}}$ ) with  $\Omega_m \equiv \Omega_c + \Omega_b + \Omega_\nu$ .

Using this chain we have reproduced the  $\sum m_\nu < 1.3 \text{ eV}$  limit, illustrated in Fig. 1. This is a histogram of the  $N = 7503$  values of  $\sum m_\nu \equiv M_\nu$  in the MCMC chain weighted by the weights  $w_{\text{CMB}}$  given in the chain. The 95% confidence limit on  $\sum m_\nu$ , which we denote as  $M_\nu^{\text{lim}}$ , is defined in the usual way as a region enclosing 95% of the histogram area:

$$.95 = \frac{\sum_{M_\nu^i < M_\nu^{\text{lim}}} w_{\text{CMB}}^i}{\sum_{i=1}^N w_{\text{CMB}}^i}, \quad (2)$$

where  $i$  is an index running through the entries in the MCMC chain.

## 3 ANALYSIS METHOD

We explore the robustness of a neutrino mass limit produced by combining the CMB with information from the galaxy power spectrum. We do this by performing the analysis using power spectra of different subsamples of galaxies, namely red and blue galaxies, and determining whether the resulting limits are consistent with each other, in the spirit of Sánchez & Cole (2008). We also test the effect of changing the range of  $k$  values used from the galaxy power spectra and using different prescriptions for the theoretical modeling of the nonlinear power spectra.

### 3.1 Calculating power spectra and uncertainties

Power spectra were calculated for the red, blue and combined catalogs using the Fourier method of Feldman et al.

<sup>1</sup> <http://lambda.gsfc.nasa.gov>

(1994), as applied by Percival et al. (2010). In this method a weighted galaxy over-density field is defined and Fourier transformed, then the spherically averaged power is measured. The shot noise due to the discreteness of the galaxy locations is subtracted, assuming the galaxies are a Poisson sampling of the density distribution. We use the luminosity (but not colour) dependent galaxy weights advocated by Percival et al. (2004). These will at least partially correct for power spectrum shape changes caused by variations in the galaxy bias over the redshift range of the survey due to flux-limited selection and galaxy evolution.

The power spectrum for the combined catalog is not independent of the red and blue catalogs since it includes the same galaxies. The all-galaxy power spectrum  $P_{\text{all}}(k)$  is related to the red and blue galaxy power spectra  $P_{\text{rr}}(k)$  and  $P_{\text{bb}}(k)$  by

$$P_{\text{all}}(k) = f_r^2 P_{\text{rr}}(k) + 2f_r f_b P_{\text{rb}}(k) + f_b^2 P_{\text{bb}}(k)$$

where  $f_r$  and  $f_b$  are the fractions of red and blue galaxies in the sample ( $f_r + f_b = 1$ ) and  $P_{\text{rb}}(k)$  is the cross power spectrum between red and blue galaxies. Thus  $P_{\text{all}}(k)$  contains the information from the two subsample power spectra plus the cross power spectrum.

Because of the survey mask (both angular and radial), the measured power spectrum is a convolution of the true power spectrum (Hauser & Peebles 1973; Peebles 1980; Percival et al. 2001). A discretized window function was used to quickly perform this convolution, as described in Percival et al. (2007). In order to calculate the covariances between the power spectrum band-powers, we have created 10 000 Log-Normal (LN) density fields (Coles et al. 1999; Cole et al. 2005) with a power spectrum for a flat  $\Lambda$ CDM cosmology with  $\theta^i = (\Omega_\Lambda = 0.7, \Omega_b/\Omega_m = 0.15, h = 0.7, n_s = 1, \sum m_\nu = 0)$ , and normalisation matched to the amplitude of the measured power.

From each LN density field  $\delta(\mathbf{x})$ , we draw red, blue, and combined galaxy catalogues as Poisson samplings matched to the galaxy bias and spatial distribution of the SDSS-II samples. That is, the mean  $\lambda(\mathbf{x})$  of the Poisson distribution is given by  $\lambda(\mathbf{x}) = \bar{n}(\mathbf{x})(1 + b\delta(\mathbf{x}))$ , where  $\bar{n}(\mathbf{x})$  is the mean density including the effects of the survey mask and  $b$  is the linear galaxy bias at large scales ( $k < 0.1 h \text{Mpc}^{-1}$ ) for the red and blue galaxy samples. Catalogues were calculated on a  $(512)^3$  grid with box length  $4000 h^{-1} \text{Mpc}$ . Unlike N-body simulations, these mock catalogues do not model the growth of structure, but instead return a density field with a log-normal distribution, similar to that seen in the real data. The mock catalogues also do not include redshift space distortions. Power spectra for the mock catalogues were calculated following the same method used for the SDSS-II data and were used to compute covariance matrices for each subsample.

A subset of 200 of the mock catalogue power spectra was also used to estimate the expected sensitivity of the neutrino mass limit. We do this by applying our analysis described in Section 3.4 to the mock power spectra and define a range using the mean  $\pm$  one standard deviation of the 95% CL limits on  $\sum m_\nu$  from the mocks. Because the mock catalogues have  $\sum m_\nu = 0$  and linear bias, the expected sensitivity range is the range in which we would expect to measure the neutrino mass limit assuming that the neutrino mass were equal to zero and that we understood bias per-

fectly. This provides a baseline for interpreting the neutrino mass limits determined from the actual data.

### 3.2 Models for galaxy bias and nonlinear evolution

Our starting point for theoretical modeling is the linear power spectrum  $P_{\text{lin}}(k, z)$  calculated using CAMB<sup>2</sup> for our set of cosmological parameters  $\theta^i \equiv (\Omega_\Lambda, \Omega_b/\Omega_m, h, \sigma_8, n_s, \sum m_\nu)$ . We evaluate  $P_{\text{lin}}(k, z)$  at the median redshift of each galaxy sample ( $z = 0.111$  for red,  $z = 0.085$  for blue, and  $z = 0.099$  for all galaxies) and drop the explicit dependence on  $z$  in our power spectra for notational convenience.

We consider twelve different models for converting  $P_{\text{lin}}(k, z)$  into a galaxy power spectrum. The first six models represent the typical models used in previous cosmological analyses of the neutrino mass and have either one or two additional free parameters,  $b$  and a free parameter that controls the amplitude of the non-linear change in shape between galaxy and linear matter power spectrum, which can take on different values for different galaxy subsamples.

For our remaining six models, we explore variations on new models for the matter power spectrum including a contribution from massive neutrinos, based on perturbation theory described in Saito et al. (2008, 2009); Taruya et al. (2009). For this theory, the baseline model is

$$P_{\text{pt}}(k) \equiv f_{\text{cb}} P_{\text{1loop}}^{\text{cb}}(k) + 2f_{\text{cb}} f_\nu P_{\text{lin}}^{\text{cb}\nu}(k) + f_\nu^2 P_{\text{lin}}^\nu(k), \quad (3)$$

where  $f_{\text{cb}}$  and  $f_\nu$  are the mass fractions of cold dark matter plus baryons and neutrinos respectively,  $P_{\text{lin}}^\nu(k)$  is the linear theory power spectrum for neutrinos only,  $P_{\text{lin}}^{\text{cb}\nu}(k)$  is the linear theory cross power spectrum between cold dark matter plus baryons and neutrinos, and  $P_{\text{1loop}}^{\text{cb}}(k)$  is the nonlinear power spectrum of cold dark matter plus baryons computed to one loop in perturbation theory, which has been studied extensively in the literature (e.g., Juszkiewicz 1981; Makino et al. 1992; Jain & Bertschinger 1994; Scoccimarro & Frieman 1996; Heavens et al. 1998). Here we use

$$P_{\text{1loop}}^{\text{cb}}(k) \equiv P_{\text{lin}}^{\text{cb}}(k) + P_{(22)}^{\text{cb}}(k) + P_{(13)}^{\text{cb}}(k), \quad (4)$$

where  $P_{(22)}^{\text{cb}}(k)$  and  $P_{(13)}^{\text{cb}}(k)$  are the approximations to the one-loop correction spectra given by equations (32) and (36) in Saito et al. (2009). If we replace  $P_{\text{1loop}}^{\text{cb}}(k)$  by  $P_{\text{lin}}^{\text{cb}}(k)$  in equation (3), the expression for  $P_{\text{pt}}(k)$  reduces to  $P_{\text{lin}}(k)$ . The motivation for this model is that while cold dark matter and baryon perturbations start to behave non-linearly at  $k \gtrsim 0.1 h \text{Mpc}^{-1}$ , perturbations of the neutrino density will tend to remain mostly linear due to the large velocity dispersion of the neutrinos. Similar models have been explored by Hannestad et al. (2006); Ichiki et al. (2009) and further improved by Wong (2008); Lesgourgues et al. (2009).

The twelve models used in this analysis are as follows:

(i) The simplest model for the galaxy power spectrum is that of constant linear bias of this linear power spectrum:

$$P_{\text{gal}}(k) = b^2 P_{\text{lin}}(k), \quad (5)$$

<sup>2</sup> <http://camb.info/>

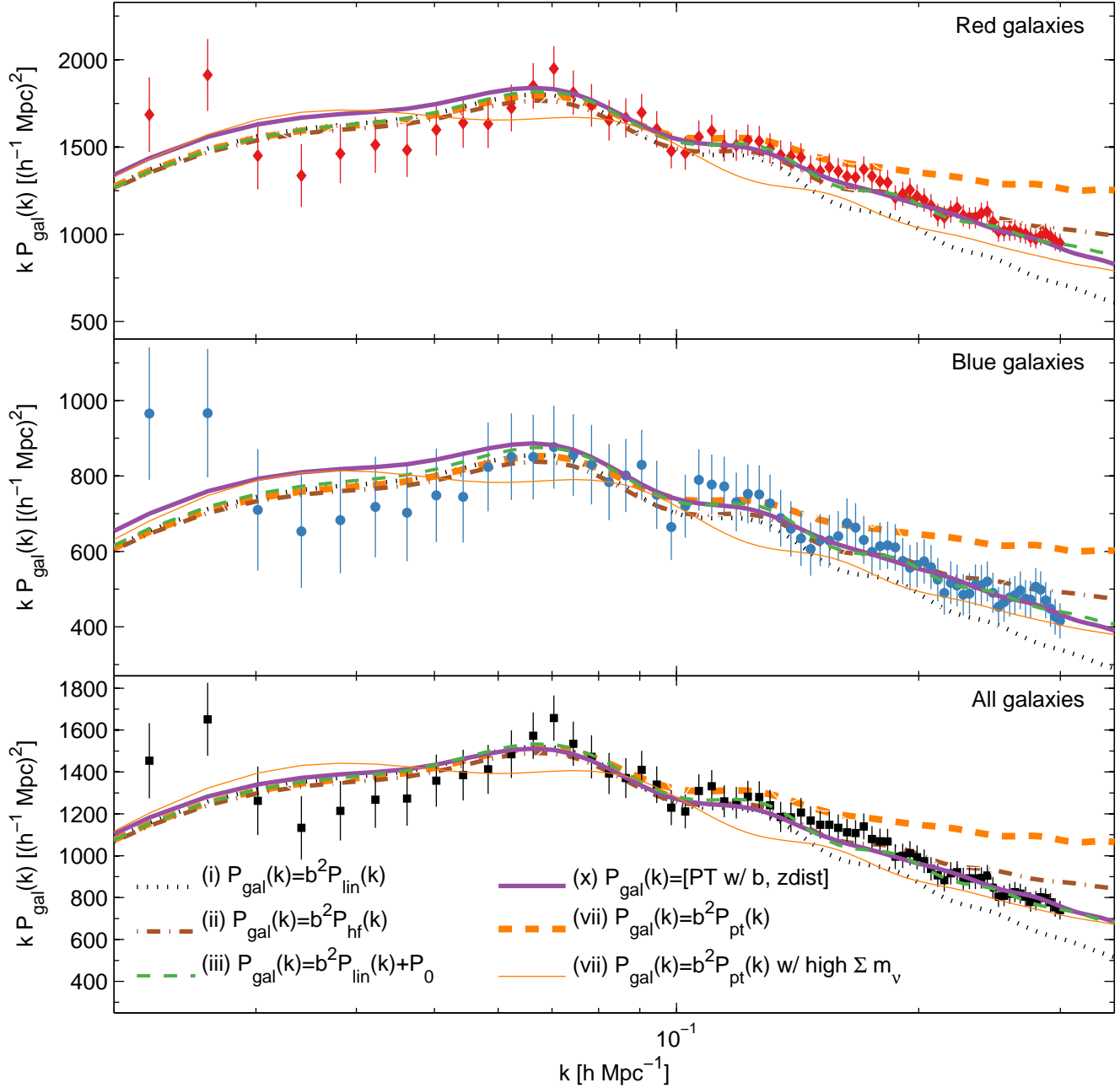


**Figure 2.** Measured SDSS-II DR7 power spectra for red (top panel), blue (middle panel), and all (bottom panel) galaxies compared to several theoretical models. All curves plotted with thick lines use the cosmology from the WMAP5  $\Lambda\text{CDM} + \Sigma m_\nu$  MCMC chain that yields the maximum likelihood for WMAP5 only. Models (iii) and (x) are plotted with the bias parameters that give the best fit to the  $P(k)$  data shown for  $k < 0.3 h\text{Mpc}^{-1}$  and models (i), (ii), and (vii) are plotted with the best-fit  $b$  for the data shown at  $k < 0.1 h\text{Mpc}^{-1}$  to better illustrate the different behaviours at small scales. The thin orange line and the thick dashed orange line both use model (vii), but the thin orange line uses cosmology and bias parameters that give the maximum likelihood to the  $P(k)$  data at  $k < 0.3 h\text{Mpc}^{-1}$  for the  $P_{\text{gal}}(k) = b^2 P_{\text{pt}}(k)$  model – this cosmology has a high value of with a high  $\Sigma m_\nu$  and fits the data better than the thick dotted orange line (though not as well as models (iii) and (x)). This illustrates how increasing the neutrino mass can lead to a better fit for some models. See text for more detailed discussion.

where the bias  $b$  is allowed to take on different values for different galaxy subsamples.

(ii) Our second model replaces the linear matter power spectrum with the Halofit nonlinear transformation (Smith et al. 2003), which we denote  $P_{\text{hf}}(k)$ :

$$P_{\text{gal}}(k) = b^2 P_{\text{hf}}(k). \quad (6)$$

(iii) For the next model we add one more free parameter to model (i) as an additive constant term:

$$P_{\text{gal}}(k) = b^2 P_{\text{lin}}(k) + P_0. \quad (7)$$

The  $P_0$  parameter has a physical basis: it represents a change in the shot noise. If galaxies are not a Poisson sample of

the matter distribution, our power spectrum calculation will subtract the shot noise imperfectly. Non-Poisson shot noise is a generic prediction of the halo model (Seljak 2000): in this context,  $P_0$  is an approximation to the one-halo contribution to the power spectrum. This model was proposed by Seljak (2001); Schulz & White (2006); Guzik et al. (2007) and has been explored by, e.g., Hamann et al. (2008); Cresswell & Percival (2009). We refer to it as the P-model.

(iv) We can do the same for model (i), giving

$$P_{\text{gal}}(k) = b^2 P_{\text{hf}}(k) + P_0. \quad (8)$$

(v) As an alternative to the P-model, we also test the Q-model put forth by Cole et al. (2005), which adds a different free parameter  $Q$  to “correct” for unknown scale-dependent galaxy bias and redshift space distortions:

$$P_{\text{gal}}(k) = b^2 \frac{1 + Qk^2}{1 + 1.4k} P_{\text{lin}}(k). \quad (9)$$

Cole et al. (2005) test and calibrate this model with N-body simulations populated by a semi-analytic galaxy formation model under the assumption of massless neutrinos – its validity in the massive neutrino case has not been tested in detail. We include it here to facilitate comparison with other analyses that adopt this model, e.g., Tegmark et al. (2006).

(vi) It is not clear that either the P-model or the Q-model correctly accounts for the damping of the Baryon Acoustic Oscillations (BAO) by the non-linear structure growth and redshift-space distortions. In order to confirm that this is not a big effect for neutrino mass constraints, we also consider a model with

$$P_{\text{gal}}(k) = b^2 \frac{1 + Qk^2}{1 + 1.4k} P_{\text{dw}}(k), \quad (10)$$

where  $P_{\text{dw}}(k)$  is the “dewiggled” power spectrum calculated in the manner of Tegmark et al. (2006) that accounts for the non-linear damping of the BAO:

$$P_{\text{dw}}(k) = W(k) P_{\text{lin}}(k) + [1 - W(k)] P_{\text{nowiggle}}(k), \quad (11)$$

where  $W(k) \equiv e^{-(k/k_*)^2/2}$  and  $P_{\text{nowiggle}}(k)$  represents a smooth power spectrum without BAO that we calculate using a smooth b-spline fit to  $k^{1.5} P_{\text{lin}}(k)$  with eight nodes equally spaced in  $\log(k)$  from  $k = 0.007$  to  $k = 0.7 \text{ Mpc}^{-1}$ . This is similar to the method used in Reid et al. (2010b) for massive neutrino models. Following Tegmark et al. (2006) we define  $k_* \equiv \sigma_{\perp}^{-2/3} \sigma_{\parallel}^{-1/3} (A_s/0.6841)^{-1/2}$  with  $\sigma_{\perp}$  and  $\sigma_{\parallel}$  given by equations (12) and (13) in Eisenstein et al. (2007).

(vii) We now consider a model where we replace the linear matter power spectrum in (i), with  $P_{\text{pt}}(k)$  given by equation (3):

$$P_{\text{gal}}(k) = b^2 P_{\text{pt}}(k), \quad (12)$$

(viii) We can do the same for the P-model (iii)

$$P_{\text{gal}}(k) = b^2 P_{\text{pt}}(k) + P_0. \quad (13)$$

(ix) For our next model, we use an extension of  $P_{\text{pt}}(k)$  to include nonlinear galaxy bias. Starting from the assumption of local deterministic nonlinear bias, Saito et al. (2009) derive an expression for  $P_{\text{gal}}(k)$  using the perturbation theory

methods from McDonald (2006); Jeong & Komatsu (2009) involving one new free parameter  $b_2$ :

$$P_{\text{gal}}(k) = b^2 [P_{\text{pt}}(k) + b_2 P_{b_2, \delta}(k) + b_2^2 P_{b_2 22}(k)] + P_0, \quad (14)$$

where  $P_{b_2, \delta}(k)$  and  $P_{b_2 22}(k)$  are given by equation (41) in Saito et al. (2009) and  $b_2$  is a third free parameter allowed to take on different values for different galaxy subsamples. We label this model as “PT with  $b, P_0, b_2$ ” in our results.

(x) Next we consider extending the perturbations theory analysis into redshift-space following Taruya et al. (2009) and applying the redshift space distortion model of Scoccimarro (2004). According to Scoccimarro (2004), the redshift space power spectrum of matter can be modeled by

$$P_{\text{zdist}}(k, \mu) = [P_{\delta\delta}(k) + 2f\mu^2 P_{\delta\theta}(k) + f^2 \mu^4 P_{\theta\theta}(k)] \times \exp(- (f\mu k \sigma_v)^2), \quad (15)$$

where  $f \equiv d \ln D / d \ln a$  ( $a$  being the scale factor and  $D$  being the growth factor) is the linear growth rate,  $\mu \equiv \hat{\mathbf{k}} \cdot \hat{\mathbf{z}}$  is the cosine of the angle between the wavevector  $\mathbf{k}$  and the line of sight  $\mathbf{z}$ .  $P_{\delta\delta}(k)$  and  $P_{\theta\theta}(k)$  are nonlinear density and velocity power spectra, and  $P_{\delta\theta}(k)$  is the density-velocity cross-power spectrum, all calculated with one-loop perturbation theory as defined in equations (63-65) in Scoccimarro (2004). The one-dimensional velocity dispersion  $\sigma_v$  is defined as

$$\sigma_v^2 \equiv \frac{1}{3} \int \frac{d^3 \mathbf{q}}{(2\pi)^3} \frac{P_{\theta\theta}(q)}{q^2}. \quad (16)$$

Following Saito et al. (2009), we calculate  $P_{\delta\delta}(k)$ ,  $P_{\theta\theta}(k)$  and  $P_{\delta\theta}(k)$  in the same manner as in equation (3): we apply the one-loop corrections to the cold dark matter plus baryon portion of the power spectrum and leave the neutrino power spectrum linear. Thus  $P_{\delta\delta, \text{pt}}(k) = P_{\text{pt}}(k)$  as defined in equation (3), and  $P_{\theta\theta, \text{pt}}(k)$  and  $P_{\delta\theta, \text{pt}}(k)$  are defined analogously.

To model the angle-averaged redshift space power spectrum, which is what our data actually represents, we integrate equation (15) over  $\mu$ :

$$P_{\text{zdist}}(k) = A_0(k) P_{\text{pt}}(k) + 2f A_2(k) P_{\delta\theta, \text{pt}}(k) + f^2 A_4(k) P_{\theta\theta, \text{pt}}(k) \quad (17)$$

where  $A_n(k)$  are moments of the Gaussian term in equation (3):

$$A_n(k) \equiv \int_{-1}^1 d\mu \mu^n \exp(- (f\mu k \sigma_v)^2) \quad (18)$$

We model the galaxy power spectrum in redshift space with linear bias by using bias  $b$  for the density terms and no bias for the velocity terms, giving

$$P_{\text{gal}}(k) = A_0(k) b^2 P_{\text{pt}}(k) + 2f A_2(k) b P_{\delta\theta, \text{pt}}(k) + f^2 A_4(k) P_{\theta\theta, \text{pt}}(k) \quad (19)$$

This model is labeled as “PT with  $b, \text{zdist}$ ”.

(xi) The P-model under this redshift space distortion model becomes

$$P_{\text{gal}}(k) = A_0(k) [b^2 P_{\text{pt}}(k) + P_0] + 2f A_2(k) b P_{\delta\theta, \text{pt}}(k) + f^2 A_4(k) P_{\theta\theta, \text{pt}}(k) \quad (20)$$

which we label as “PT with  $b, P_0, \text{zdist}$ ”.

(xii) Finally, we combine the nonlinear bias model of equation (14) with the redshift space distortion model to give

$$P_{\text{gal}}(k) = A_0(k) \{ b^2 [P_{\text{pt}}(k) + b_2 P_{b_2, \delta}(k) + b_2^2 P_{b_2 2}(k)] + P_0 \} + 2A_2(k) b [f P_{\delta \theta, \text{pt}}(k) + b_2 P_{b_2 v}(k)] + f^2 A_4(k) P_{\theta \theta, \text{pt}}(k), \quad (21)$$

which we label as ‘‘PT with  $b$ ,  $P_0$ ,  $b_2$ ,  $\text{zdist}$ ’’.  $P_{b_2 v}(k)$  is defined analogously to  $P_{b_2, \delta}(k)$  by replacing the density kernel with the velocity kernel in equation (41) in Saito et al. (2009).

We calculate all of the various power spectra in equations (19), (20), and (21) using a modified version of CAMB provided by Saito (private communication). Note that our redshift space distortion model does not add any new free parameters:  $P_{\text{zdist}}(k)$  is fully defined by equation (17) once  $P_{\text{lin}}(k)$  has been determined.

Models (i), (ii), (vii) and (x) have one free bias parameter  $b$ , models (iii), (iv), (v), (vi), (viii) and (xi) have two free bias parameters ( $b$  and either  $P_0$  or  $Q$ ), and models (ix) and (xii) have three free bias parameters ( $b$ ,  $P_0$  and  $b_2$ ). These free parameters are all allowed to take on different values for the red and blue galaxy subsamples.

To illustrate some of the main features of these models, we plot a subset of them with our power spectrum data in Fig. 2. For all but one of the curves plotted, we use the parameter set from the  $\Lambda\text{CDM} + \sum m_\nu$  MCMC chain that gives the maximum likelihood for WMAP5 only:  $\theta^i \equiv (\Omega_\Lambda = 0.7263, \Omega_b/\Omega_m = 0.1666, h = 0.7050, \sigma_8 = 0.8065, n_s = 0.9580, \sum m_\nu = 0.0287 \text{ eV})$ . The remaining curve is plotted with the parameter set from the MCMC chain giving the maximum likelihood the all-galaxy  $P(k)$  data using the  $b^2 P_{\text{pt}}(k)$  model:  $\theta^i \equiv (\Omega_\Lambda = 0.5168, \Omega_b/\Omega_m = 0.1392, h = 0.5596, \sigma_8 = 0.5459, n_s = 0.9140, \sum m_\nu = 1.34 \text{ eV})$ .

Figure 2 shows that model (x) (PT with  $b$ ,  $\text{zdist}$ ) closely mimics model (iii) (the P-model) for the maximum likelihood WMAP5 cosmology and in fact fits the data just as well with one less free parameter. The other models plotted show different shapes at small scales, with the  $b^2 P_{\text{lin}}(k)$  model underestimating the small-scale power and  $b^2 P_{\text{pt}}(k)$  overestimating it. The  $b^2 P_{\text{pt}}(k)$  curve for the high  $\sum m_\nu$  cosmology gives a shape closer to the data than the same model with WMAP5 cosmology because it compensates for the excess of small-scale power by adding more massive neutrinos that damp it out. This means that a model of bias or nonlinearity that overestimates the small-scale power could potentially lead to a ‘‘false positive’’ measurement of neutrino mass. The effect of this can be seen quantitatively in our results.

### 3.3 Calculating the galaxy power spectrum likelihood

To compare our theoretical models to the power spectrum data, we convolve our model  $P_{\text{gal}}(k)$  with the window function  $W(k_j, k_n)$  discussed in Section 3.1, where  $k_j$  are the central wavenumbers of the observed bandpowers and  $k_n$  are the wavenumbers at which we evaluate the theory power spectra. Following Reid et al. (2010b), we define the convolved theory power spectrum by

$$P_{\text{gal,win}}(k_j, \theta, \theta_b) = \sum_n W(k_j, k_n) P_{\text{gal}}(k_n/a_{\text{scl}}, \theta, \theta_b) / a_{\text{scl}}^3 - W(k_j, 0) \quad (22)$$

where  $\theta$  are the cosmological parameters defined in Section 2.2 and  $\theta_b$  are the galaxy bias parameters for the model being used:  $b$  and possibly  $b_2$  and  $P_0$  or  $Q$ .

Equation (22) includes two very small adjustments: the  $W(k_j, 0)$  term accounts for the integral constraint issue from estimating the average galaxy density from the sample itself (Percival et al. 2007; Reid et al. 2010b), and the  $a_{\text{scl}}$  factors adjust for the fact that we use one fiducial cosmology to convert our galaxy redshifts into distances rather than recalculating the distances for each cosmology (Tegmark et al. 2006; Reid et al. 2010b), with

$$a_{\text{scl}} = \left[ \frac{D_A^2(z_{\text{med}}) H_{\text{fid}}(z_{\text{med}})}{[D_A^{\text{fid}}(z_{\text{med}})]^2 H(z_{\text{med}})} \right]^{1/3}, \quad (23)$$

where  $D_A$  and  $H$  are the angular diameter distance and Hubble parameter for the cosmology defined by  $\theta$ ,  $D_A^{\text{fid}}$  and  $H_{\text{fid}}$  are for the fiducial cosmology, and  $z_{\text{med}}$  is the median redshift of the galaxy sample.

The likelihood was calculated assuming that the power spectrum data are distributed as a multi-variate Gaussian distribution:

$$-2 \ln L(\theta, \theta_b) = \chi^2(\theta, \theta_b) = \sum_{jk} \Delta_j C_{jk}^{-1} \Delta_k, \quad (24)$$

where  $\Delta_j \equiv [\hat{P}_{\text{gal}}(k_j) - P_{\text{gal,win}}(k_j, \theta, \theta_b)]$ ,  $\hat{P}_{\text{gal}}(k_j)$  is the measured galaxy power spectrum, and  $C_{jk}$  is the covariance matrix calculated as described in Section 3.1.

Our final galaxy power spectrum likelihood is defined by marginalizing over the bias parameters  $\theta_b$  by integrating the likelihood over the prior distribution  $\pi(\theta_b)$ :

$$L_{P(k)}(\theta) \equiv \int d^n \theta_b L(\theta, \theta_b) \pi(\theta_b). \quad (25)$$

We use a flat prior on  $b^2$  from 0 to  $+\infty$  and flat priors on  $P_0$ ,  $b_2$ , and  $Q$  ranging from  $-\infty$  to  $+\infty$ . We perform this marginalization analytically where possible, which is the case for most of our models. For models (ix) and (xii), we have to integrate over  $b_2$  numerically, and for models (x), (xi), and (xii) (the ones including redshift space distortion) we must do the integral over  $b^2$  numerically as well.

### 3.4 Importance sampling

Because we have to evaluate the neutrino mass limit for several different power spectrum models and  $k$  cutoff values, we reduce the computational requirement by using the technique of importance sampling (Lewis & Bridle 2002): we use a fixed WMAP MCMC chain and reweight the chain entries according to the revised likelihood values calculated for the different galaxy power spectrum fits. Given an MCMC chain of parameter values  $\theta$  drawn from a likelihood distribution  $L$ , one can compute parameter constraints relative to a similar distribution  $L'$  by re-weighting the sample according to the likelihood ratios:

$$w_{L'}^i = \frac{L'(\theta^i)}{L(\theta^i)} w_L^i. \quad (26)$$

Since the CMB measurement and the galaxy power spectrum measurement are independent experiments, we can find the combined likelihood simply by multiplying the two likelihoods together:

$$L_{\text{CMB}+P(k)}^i = L_{P(k)}(\theta^i) L_{\text{CMB}}^i(\theta^i). \quad (27)$$

Thus the WMAP MCMC chain can be reweighted by

$$w_{\text{CMB}+P(k)}^i = L_{P(k)}^i(\theta^i) w_{\text{CMB}}^i, \quad (28)$$

so the 95% confidence upper limit on  $\sum m_\nu$  is the value of  $M_\nu^{\text{lim}}$  that satisfies

$$.95 = \frac{\sum_{M_\nu^i < M_\nu^{\text{lim}}} L_{P(k)}^i(\theta^i) w_{\text{CMB}}^i}{\sum_{i=1}^N L_{P(k)}^i(\theta^i) w_{\text{CMB}}^i}. \quad (29)$$

As a test of the importance sampling method, we applied it to the dark matter halo power spectrum  $\hat{P}_{\text{halo}}(k)$  derived from the DR7 Luminous Red Galaxies using the likelihood code of Reid et al. (2010b) to evaluate  $L_{P(k)}$ . Our importance sampling method yields  $\sum m_\nu < 0.64 \text{ eV}$  (95% CL) for WMAP5 +  $\hat{P}_{\text{halo}}(k)$ , which agrees within 3% to the result from Reid et al. (2010b) of  $\sum m_\nu < 0.62 \text{ eV}$ . We therefore conclude that importance sampling is sufficiently robust for the purposes of our analysis in this paper.

To summarize, the steps to calculate the neutrino mass limit from WMAP5 + galaxy power spectrum are:

(i) For each entry of cosmological parameter values in the MCMC chain, calculate a linear power spectrum  $P_{\text{lin}}(k)$  with those parameters using CAMB.

(ii) Choose a model for nonlinear evolution and bias, as described in §3.2.

(iii) Calculate likelihood of this model power spectrum using a measured galaxy power spectrum.

(iv) Marginalize over the bias parameters by integrating the resulting likelihood analytically or numerically.

(v) Use importance sampling (Lewis & Bridle 2002) to reweight the entry in the WMAP5 MCMC chain by the likelihood from the galaxy power spectrum:

$$w_{\text{CMB}+P(k)}^i = L_{P(k)}^i w_{\text{CMB}}^i \quad (30)$$

(vi) Repeat this for each entry in WMAP5 MCMC chain, and then calculate the neutrino mass limit using histograms of the MCMC chain weighted by  $w_{\text{CMB}+P(k)}$ .

## 4 RESULTS

### 4.1 Neutrino mass constraints

We have performed the above procedure using the power spectra for the full SDSS-II DR7 main sample, and for the same sample split into red and blue galaxies. For each of the three samples, we have done the calculation using power spectrum values for  $k < k_{\text{max}}$ , with  $k_{\text{max}}$  ranging from 0.06 to  $0.3 h \text{ Mpc}^{-1}$  and repeated this for each of our twelve models for bias and nonlinearities. Results for the first six models are plotted in Fig. 3, and results for the six models based on Saito et al. (2009) are plotted in Fig. 4. The neutrino limits for the all-galaxy sample typically trace the limits for the red galaxies, indicating that the red galaxies dominate the signal - this is because the red galaxies are more highly biased. Furthermore, the limits from the blue galaxy sample

tend to be larger than those from the red galaxies — this is to be expected since the measurements using the red galaxies are intrinsically more sensitive and therefore give more stringent limits. We also typically obtain weaker limits as we increase the number of free parameters used to model galaxy bias and nonlinearities, as expected.

One notable feature seen in Figs. 3 and 4 is that for the all-galaxy sample using the  $b^2 P_{\text{hf}}(k)$  model and all three galaxy samples using the  $b^2 P_{\text{pt}}(k)$  model, the neutrino limit increases sharply at the high end of our  $k_{\text{max}}$  range. To explore what is driving this, we plot the histograms for  $k_{\text{max}} = 0.3 h \text{ Mpc}^{-1}$  for the red galaxy sample using the [PT w/  $b$ ,  $z\text{dist}$ ],  $b^2 P_{\text{hf}}(k)$  and  $b^2 P_{\text{pt}}(k)$  models in Fig. 5.

The distribution for the  $b^2 P_{\text{pt}}(k)$  case clearly peaks at a non-zero neutrino mass, and a hint of a secondary peak at non-zero neutrino mass can be seen in the  $b^2 P_{\text{hf}}(k)$  histogram as well. From Fig. 2 we can see that the driving force behind this effect is that for models with no flexibility in the power spectrum shape, the differences in the amount of upturn at the high- $k$  end are compensated for by changing the cosmology instead. For the  $b^2 P_{\text{pt}}(k)$  model, the shape of the power spectrum for the best-fit WMAP5 parameters overestimates the data at high  $k$ , and increasing the neutrino mass can pull the high- $k$  end down into better agreement with the data.

We have compared the neutrino mass limits calculated from the SDSS-II data against those from 200 mock catalogues: the shaded regions in Figs. 3 & 4 contain 68% of the neutrino mass limits from mock catalogues. As discussed in Section 3.1, we would expect to measure the neutrino mass limit to be within this expected sensitivity range if the neutrino mass were equal to zero and we understood bias perfectly. They will therefore underestimate the true range of limits. Because the mock catalogues are constructed to have a power spectrum matched to  $P_{\text{lin}}(k)$  with linear bias and no redshift space distortions, we use the  $b^2 P_{\text{lin}}(k)$  model on the mock catalogues to define the expected sensitivity range for models (i), (ii), (vii), and (x) (all of the one-parameter bias models). Likewise, we use the  $b^2 P_{\text{lin}}(k) + P_0$  model for the expected sensitivity range for models (iii), (iv), (viii), and (xi) (all of the P-models), the  $b^2 (1 + Qk^2) / (1 + 1.4k) P_{\text{lin}}(k)$  model for both of the Q-models (v) and (vi), and the [PT w/  $b$ ,  $P_0$ ,  $b_2$ ] model for both of the  $b_2$  models (ix) and (xii). This correctly captures the weakening of sensitivity due to adding more free parameters but still allows for a good fit to the power spectrum built into the mocks. (Note that this is not strictly true for the Q-models as  $Q = 0$  does not reduce to  $P_{\text{lin}}(k)$ ; however, we expect the effects of this to be negligible.)

Comparing the data curves to the shaded regions in Figs. 3 and 4, we see that the results from red and blue galaxies are generally consistent with the limits predicted from the mock catalogues at the  $1\sigma$  level, which suggests that current neutrino mass limits from large scale structure are sufficiently robust to differences in bias modeling. However, the constraints from the red galaxies are systematically better than expected, while the results from the blue galaxies are systematically worse. We consider this difference further in Section 4.3.

We show our 95% confidence limits on the summed neutrino mass for each model Table 1, using both conservative ( $k_{\text{max}} < 0.12 h \text{ Mpc}^{-1}$ ) and aggressive ranges of scale



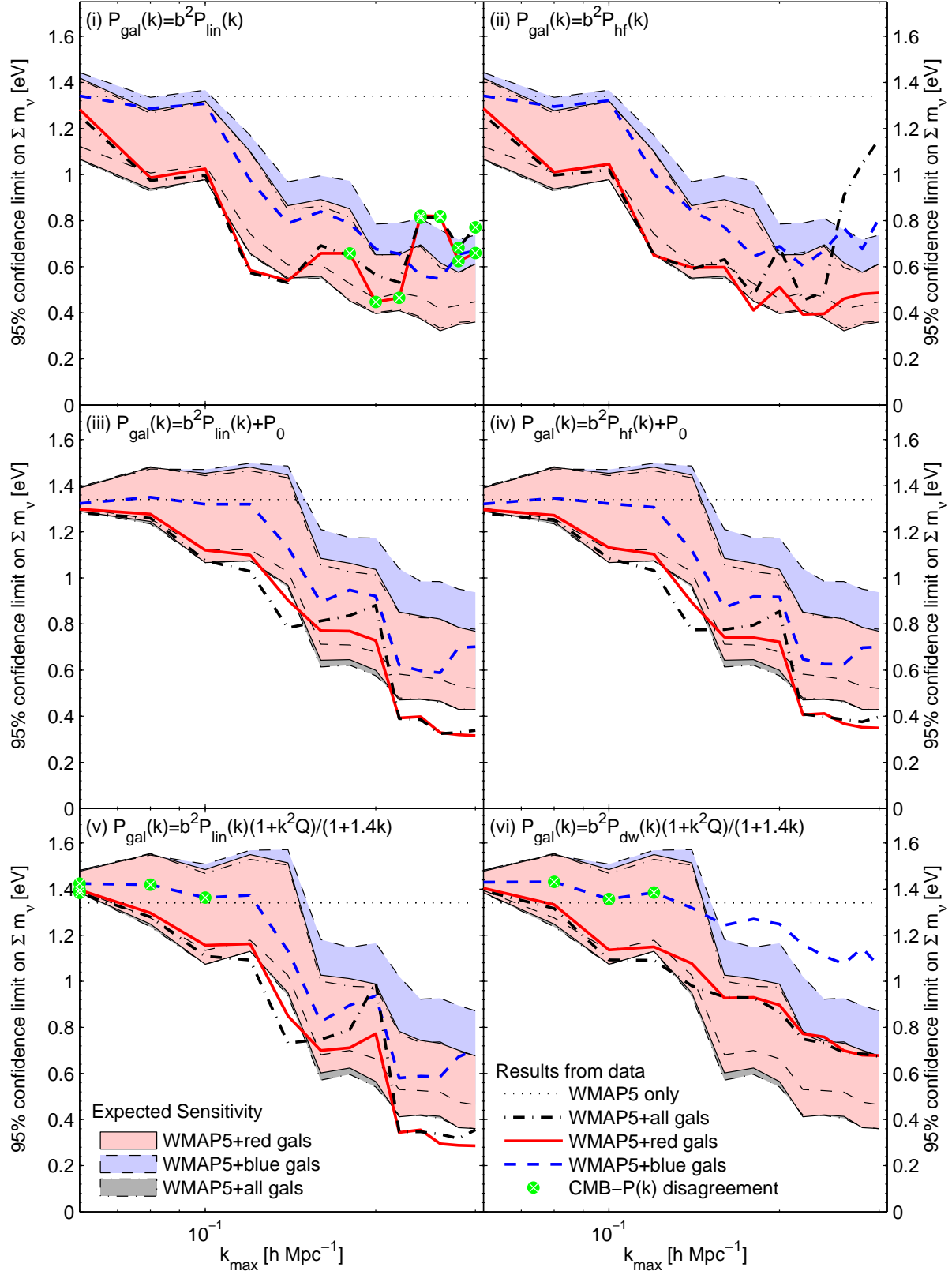


**Figure 3.** 95% CL limits on  $\Sigma m_\nu$  as determined by WMAP5 plus the SDSS-II DR7 galaxy power spectrum up to a maximum wavenumber  $k_{\text{max}}$  for bias models frequently used in the literature, e.g. Elgarøy et al. (2002); Cole et al. (2005); Tegmark et al. (2004, 2006); Hamann et al. (2008). Expected sensitivity ranges show the mean limit  $M_\nu^{\text{lim}} \pm$  one standard deviation measured from 200 mock galaxy catalogs and represent what we would expect to measure for the neutrino mass limit assuming that  $\Sigma m_\nu = 0$  and we understood the bias perfectly. Green points indicate cases where the CMB and galaxy datasets may potentially be inconsistent with each other – these points should be regarded with caution. Using data at larger  $k$  values leads to tighter limits on  $\Sigma m_\nu$  but makes the results increasingly model-dependent.

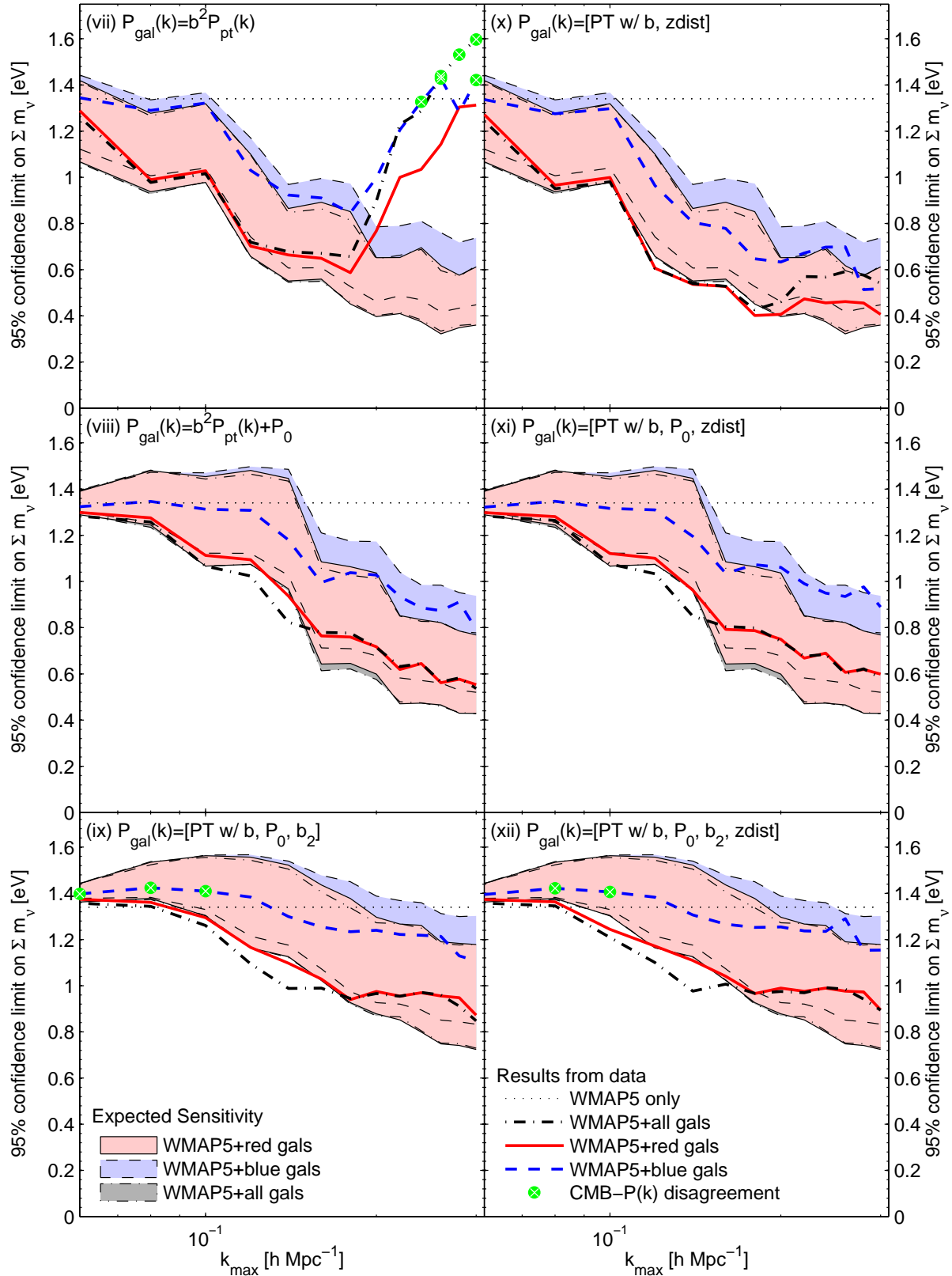


**Figure 4.** 95% CL limits on  $\Sigma m_\nu$  as determined by WMAP5 plus the SDSS-II DR7 galaxy power spectrum up to a maximum wavenumber  $k_{\text{max}}$  for bias models based on perturbation theory results from Scoccimarro (2004); Saito et al. (2008); Taruya et al. (2009). Expected sensitivity ranges show the mean limit  $M_\nu^{\text{lim}} \pm$  one standard deviation measured from 200 mock galaxy catalogs and represent what we would expect to measure for the neutrino mass limit assuming that  $\Sigma m_\nu = 0$  and we understood the bias perfectly. Green points indicate cases where the CMB and galaxy datasets may potentially be inconsistent with each other – these points should be regarded with caution. Using data at larger  $k$  values leads to tighter limits on  $\Sigma m_\nu$  but makes the results increasingly model-dependent.

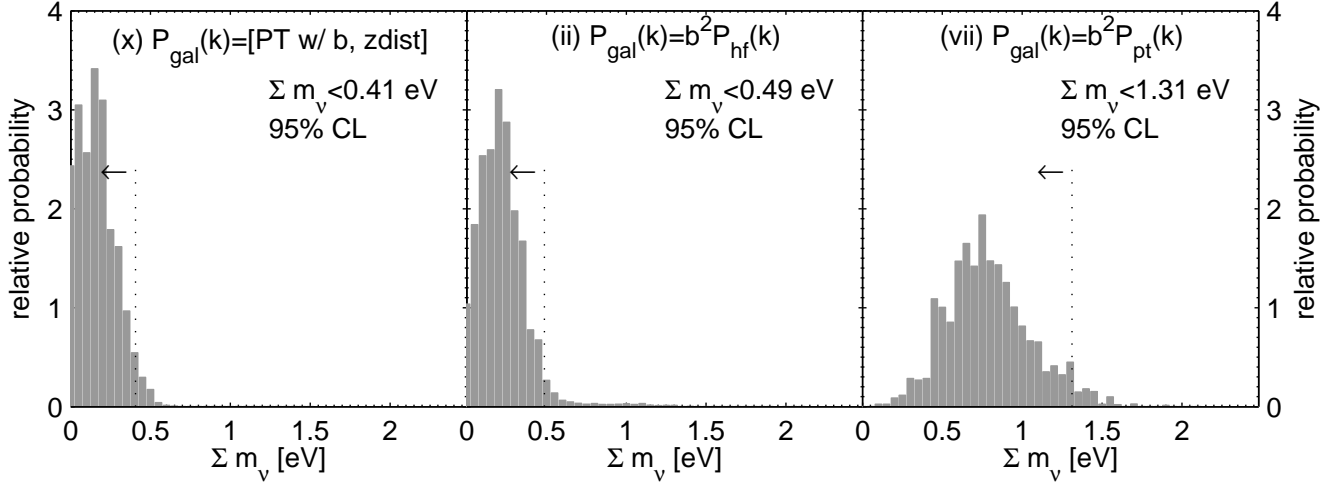


**Figure 5.** Probability distributions for  $M_\nu$  using WMAP5 +  $P(k)$  with  $k < 0.3 h \text{ Mpc}^{-1}$  for the red galaxy samples.

**Table 1.** Summary of neutrino limits, calculated to a conservative wavenumber limit  $k_{\text{max}} < 0.12 h \text{ Mpc}^{-1}$ , and to a more aggressive limit  $k_{\text{max}} < 0.2 h \text{ Mpc}^{-1}$ . Models are classified by the number of free parameters that are used to model galaxy bias.

Limits on $\sum m_\nu$ in eV at 95% CL		# of free params	Conservative ( $k_{\text{max}} < 0.12 h \text{ Mpc}^{-1}$ )			Aggressive ( $k_{\text{max}} < 0.2 h \text{ Mpc}^{-1}$ )		
Model			blue	red	all	blue	red	all
(i)	$b^2 P_{\text{lin}}(k)$	1	0.98	0.58	0.57	0.68	0.45	0.56
(ii)	$b^2 P_{\text{hf}}(k)$	1	1.00	0.65	0.65	0.69	0.51	0.68
(iii)	$b^2 P_{\text{lin}}(k) + P_0$	2	1.32	1.10	1.03	0.92	0.73	0.88
(iv)	$b^2 P_{\text{hf}}(k) + P_0$	2	1.31	1.10	1.03	0.92	0.72	0.85
(v)	$b^2 (1 + Qk^2) / (1 + 1.4k) P_{\text{lin}}(k)$	2	1.37	1.16	1.09	0.94	0.77	0.99
(vi)	$b^2 (1 + Qk^2) / (1 + 1.4k) P_{\text{dw}}(k)$	2	1.39	1.15	1.09	1.25	0.90	0.87
(vii)	$b^2 P_{\text{pt}}(k)$	1	1.03	0.70	0.72	1.00	0.77	0.90
(viii)	$b^2 P_{\text{pt}}(k) + P_0$	2	1.31	1.09	1.02	1.03	0.72	0.71
(ix)	PT with $b, P_0, b_2$	3	1.38	1.17	1.09	1.24	0.97	0.97
(x)	PT with $b, \text{zdist}$	1	0.96	0.61	0.61	0.63	0.41	0.46
(xi)	PT with $b, P_0, \text{zdist}$	2	1.31	1.10	1.03	1.06	0.75	0.74
(xii)	PT with $b, P_0, b_2, \text{zdist}$	3	1.38	1.17	1.10	1.25	0.99	0.97

( $k_{\text{max}} < 0.2 h \text{ Mpc}^{-1}$ ). The effect of the number of free parameters in the model (excluding the effect of neutrinos) clearly has a strong effect on the recovered constraint. This is discussed further in Section 5.

## 4.2 Consistency between CMB and LSS data

When combining results from independent datasets such as our combination of CMB and galaxy power spectrum data, it is important to check that they are consistent with each other under the model. If the galaxy power spectrum is not fit well by any set of parameters that has a reasonably high likelihood with respect to the CMB data, results obtained by combining them will be meaningless. Marshall et al. (2006) details a method to determine whether multiple datasets are consistent: compute the ratio of Bayesian evidences for two hypotheses  $H_0$  and  $H_1$ , where  $H_0$  is ‘‘There is one set of parameters defining one global model that describes all datasets,’’ and  $H_1$  is ‘‘There is a different set of parameters that describes each dataset.’’

For two independent datasets  $\mathbf{d}_1$  and  $\mathbf{d}_2$ , this ratio is

(see equation (3) of Marshall et al. (2006))

$$R \equiv \frac{\Pr(\mathbf{d}_1, \mathbf{d}_2 | H_0)}{\Pr(\mathbf{d}_1 | H_1) \Pr(\mathbf{d}_2 | H_1)}. \quad (31)$$

Because calculating the evidence requires integrating over the prior distribution for all of the parameters of the model, it is computationally difficult to calculate. Motivated by Kass & Raftery (1995), we define an approximation to the evidence that can be easily computed from an MCMC chain:

$$\hat{\Pr}(\mathbf{d}_1) \equiv \left\{ \frac{\sum_{i=1}^N w_i^i [\Pr(\mathbf{d}_1 | \boldsymbol{\theta}^i)]^{-1}}{\sum_{i=1}^N w_i^i} \right\}^{-1} \quad (32)$$

This is the harmonic mean of the likelihood values in the MCMC chain and can be derived following Kass & Raftery (1995) by using importance sampling: since the MCMC chain samples the posterior distribution, we can approximate an integral of  $\Pr(\mathbf{d}_1 | \boldsymbol{\theta}^i)$  over the prior distribution with a sum over the MCMC chain by reweighting using equation (26) with  $L'$  equal to the prior distribution  $\pi(\boldsymbol{\theta}^i)$  and  $L$  equal to the posterior distribution  $\Pr(\boldsymbol{\theta}^i | \mathbf{d}_1) = \Pr(\mathbf{d}_1 | \boldsymbol{\theta}^i) \pi(\boldsymbol{\theta}^i) / \Pr(\mathbf{d}_1)$ . (Kass & Raftery 1995) indicate that while this quantity can be unstable in some cases, it

is typically accurate enough for making rough categorizations, which is how we use it here.

Following this same idea, we derive an approximation for  $R$  in the case where we have an MCMC chain for  $\mathbf{d}_1$  and are using importance sampling to combine  $\mathbf{d}_1$  and  $\mathbf{d}_2$ , as we describe in §(3.4) for  $\mathbf{d}_1 = \text{WMAP5}$  and  $\mathbf{d}_2 = P_{\text{gal}}(k)$ :

$$\hat{R} \equiv \frac{\left\{ \sum_{i=1}^N w_{1+2}^i \right\} / \left\{ \sum_{i=1}^N w_{1+2}^i [\text{Pr}(\mathbf{d}_1 | \boldsymbol{\theta}^i)]^{-1} \right\}}{\left\{ \sum_{i=1}^N w_1^i \right\} / \left\{ \sum_{i=1}^N w_1^i [\text{Pr}(\mathbf{d}_1 | \boldsymbol{\theta}^i)]^{-1} \right\}}, \quad (33)$$

where  $w_{1+2}^i$  is given, e.g., by equation (28). This is quite similar to the heuristic approach proposed by Lewis & Bridle (2002) of comparing the mean likelihood of the samples where the posterior distributions overlap to the mean likelihood under the original posterior: here we have simply replaced the mean by the harmonic mean. Following Marshall et al. (2006), we interpret a value of  $\hat{R} > 1$  as indicating that the null hypothesis  $H_0$  of a global parameter set is favored over  $H_1$  with a separate parameter set for each data set. Conversely,  $\hat{R} < 1$  indicates that  $H_1$  is favored. Obtaining a value of  $\hat{R} < 1$  does not automatically guarantee that the datasets disagree, but it is an indicator that a possible mismatch between the datasets should be investigated further.

In this analysis we use  $\hat{R}$  as a conservative ‘‘warning label’’: we mark models where  $\hat{R} < 1$  as an indication that we should proceed with caution in interpreting the results since there may be disagreement between WMAP5 and  $P_{\text{gal}}(k)$  under these models. These points are clearly marked in Figs. 3 & 4. In particular, this warning label applies to the points at the high  $k_{\text{max}}$  end of the  $b^2 P_{\text{pt}}(k)$  results where the measured limits from the combined datasets are higher than the WMAP5 only limit. This suggests that applying such a consistency check to future datasets could avoid a spurious detection of neutrino mass caused by an incorrect bias model.

### 4.3 Comparison between results from blue and red galaxies

To display these effects more clearly, and include the correlations between the blue and red galaxy samples (caused by the overlapping volume covered), we plot the difference between the neutrino mass limits from red and blue galaxies as compared to the expected range from the mock catalogs in Fig. 6. To define the expected range, we compute the difference between the neutrino limits derived from the mock blue and red galaxy samples drawn from the same mock LN density distribution. Then we find the mean and standard deviation of this difference over the 200 mocks, and plot the expected range as the mean  $\pm$  one standard deviation. This accounts for correlations between the red and blue galaxy samples due to being drawn from the same underlying distribution.

Figure 6 shows that the difference between the blue and red galaxy limits is consistent at approximately the  $1\sigma$  level, compared with the expected range for nearly all of the different bias models the entire  $k_{\text{max}}$  range tested. Red galaxy limits are systematically higher than those from the blue galaxies, even after accounting for the expected difference in sensitivity, but the significance of this is low.

## 5 CONCLUSIONS

We have performed a quantitative analysis considering how large-scale structure neutrino mass limits derived from galaxy surveys depend on our ability to model non-linear effects such as galaxy bias and redshift-space distortions. Galaxies form a bimodal distribution in colour and can be split into red and blue galaxies. These populations cluster in very different ways, with red galaxies being more strongly clustered on large scales than blue (Norberg et al. 2002; Tegmark et al. 2004; Wild et al. 2005; Collister & Lahav 2005; Swanson et al. 2008), and have a different redshift-space power spectrum shape (Cresswell & Percival 2009). Splitting into red and blue galaxies and analysing the samples separately is therefore an obvious way to empirically analyse the robustness of neutrino mass limits from galaxy clustering measurements, and we have performed this test using data from the SDSS-II DR7. To evaluate the robustness of the derived neutrino mass limits, we compare the limits to the expected sensitivity range calculated from mock Log-Normal catalogues: given the accuracy with which we have measured the galaxy power spectrum, the expected sensitivity range defines the neutrino mass limit we expect to measure if the neutrino mass were equal to zero and we understood bias perfectly.

Galaxy bias and redshift-space effects alter the measured galaxy power spectrum from that of the matter power spectrum and many different models have been suggested to account for this. To see how the choice of model affects the results for the neutrino mass limit, we have considered 12 of these models, described in Section 3.2, that span the space of currently-used models and also include new models (Saito et al. 2009; Taruya et al. 2009).

Our models can be classified by the number of galaxy bias parameters used: the simplest models use only one parameter, namely the constant linear bias  $b$  which simply renormalizes the power spectrum. More complicated models use two or three parameters to account for more complex scale-dependent effects. It is clear from the results presented in Figs. 3 & 4 that most one-parameter models break down for  $k_{\text{max}} \gtrsim 0.1 - 0.2$ , giving results beyond these limits that are inconsistent with the expected sensitivity range. The exception is model (x) (a combination of the perturbation theory model of [Saito et al. 2009] and the redshift space distortion model of [Scoccimarro 2004]), which fits impressively well with only one free parameter.

All models with two free parameters give remarkably similar results: clearly the inclusion of the extra parameter allows all of these models to mimic the broad features of galaxy bias and redshift-space distortions, leading to consistent constraints. The only 2-parameter model that stands out is the dewiggled  $Q$ -model, which is unable to fit the shape of the blue galaxy power spectrum. Three-parameter models give self-consistent but not very informative results: the inclusion of another free parameter significantly degrades our ability to see the signal of massive neutrinos. We also note that adding more free parameters increases the possibility of degeneracy with cosmological parameters, which could potentially bias the results for large  $k$  values (Saito et al. 2010).

Overall, we find constraints from the red galaxies that are slightly stronger than expected: they are at the  $1\sigma$  edge

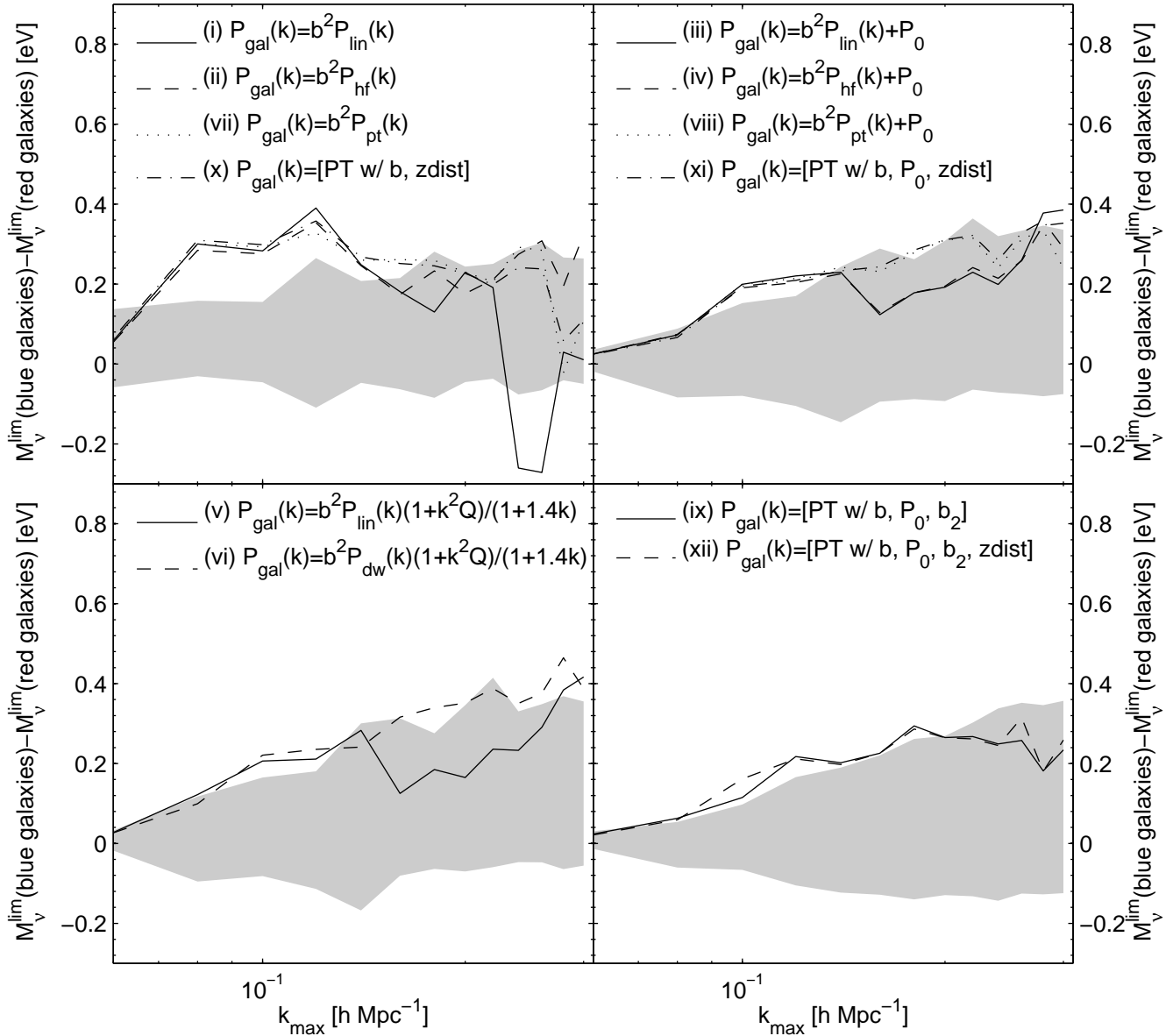


**Figure 6.** Difference between  $M_\nu^{\text{lim}}$  as determined by WMAP5 plus the SDSS-II DR7 red and blue galaxy power spectra. Shaded region shows the mean  $M_\nu^{\text{lim}}(\text{blue}) - M_\nu^{\text{lim}}(\text{red}) \pm$  one standard deviation measured from 200 mock galaxy catalogs and represent what we would expect to measure assuming that  $M_\nu = 0$  and we understood the bias perfectly.

of expected constraints, while those for blue galaxies are slightly less restrictive than expected, again approximately at the edge of the  $1\sigma$  range expected. In order to assess the significance of this potential discrepancy we need to allow for correlations between the recovered red and blue galaxy power spectra as they cover the same volume of the Universe. We account for this using mock Log-Normal catalogues, drawing overlapping red and blue mock samples from the same density fields. Figure 6 shows that the blue galaxy limit minus the red galaxy limit is slightly larger than expected: the difference in the neutrino mass result between SDSS-II red and blue galaxies is at the  $1\sigma$  limit. This matches the results shown in Figs. 3 & 4, indicating that the effect of correlations between red and blue power spectra is small.

We therefore see that, with current SDSS data, recovered neutrino mass constraints are broadly consistent for red and blue galaxies. With only these data we cannot tell if the intriguing differences between blue and red galaxies are caused by noise, or if there is an element lacking in all of the bias models we have tested. Our results indicate that current cosmological neutrino mass constraints are generally robust to astrophysical systematic effects, but that analyses of future surveys will need to treat these effects carefully in order to set convincingly tighter constraints. It is clear that being able to split a galaxy catalogue into red and blue galaxies provides an important diagnostic test of potential systematic errors, when measuring neutrino masses. When designing future surveys, it will be important to allow for such tests for systematics.

**ACKNOWLEDGMENTS**

We thank Shun Saito for kindly providing his modified CAMB code, and Filipe Abdalla, Sarah Bridle, Øystein Elgarøy, Angeliki Kiakotou, Donnacha Kirk, and Shaun Thomas for useful discussions. We thank the makers of CAMB<sup>2</sup> for making their code public, SDSS team for making their data public via <http://www.sdss.org> and the WMAP team for making their data and Monte Carlo Markov Chains public via LAMBDA<sup>1</sup>. Support for LAMBDA is provided by the NASA Office of Space Science. MS was supported by the National Science Foundation under Award No. OISE-0754357 and Award No. AST-0901965. WJP is grateful for support from the UK Science and Technology Facilities Council, the Leverhulme Trust and the European Research Council. OL acknowledges a Royal Society Wolfson Research Merit Award and an Erna & Jakob Michael Visiting Professorship at the Weizmann Institute of Science.

**REFERENCES**

- Abazajian K. N., et al., 2009, *ApJS*, 182, 543  
 Abbott T. M. C., et al., 2006, in Stepp L. M., ed., *Proc. SPIE Vol. 6267, Ground-based and Airborne Telescopes*. SPIE, Bellingham, p. 62673M  
 Abell P. A., et al., 2009, preprint (arXiv:0912.0201)  
 Ahmad Q. R., et al., 2002, *Physical Review Letters*, 89, 011301  
 Ashie Y., et al., 2005, *Phys. Rev. D*, 71, 112005  
 Blanton M. R., et al., 2003a, *AJ*, 125, 2348  
 Blanton M. R., Lin H., Lupton R. H., Maley F. M., Young N., Zehavi I., Loveday J., 2003b, *AJ*, 125, 2276  
 Casas-Miranda R., Mo H. J., Sheth R. K., Boerner G., 2002, *MNRAS*, 333, 730  
 Cole S., et al., 2005, *MNRAS*, 362, 505  
 Coles P., Melott A. L., Munshi D., 1999, *ApJ*, 521, L5  
 Collister A. A., Lahav O., 2005, *MNRAS*, 361, 415  
 Cresswell J. G., Percival W. J., 2009, *MNRAS*, 392, 682  
 Davis M., Geller M. J., 1976, *ApJ*, 208, 13  
 Davis R., 1996, *Nuclear Physics B Proceedings Supplements*, 48, 284  
 Dressler A., 1980, *ApJ*, 236, 351  
 Dunkley J., et al., 2009, *ApJS*, 180, 306  
 Eisenstein D. J., Seo H., White M., 2007, *ApJ*, 664, 660  
 Elgarøy Ø., et al., 2002, *Physical Review Letters*, 89, 061301  
 Elgarøy Ø., Lahav O., 2005, *New Journal of Physics*, 7, 61  
 Feldman H. A., Kaiser N., Peacock J. A., 1994, *ApJ*, 426, 23  
 Fukuda Y., et al., 1998, *Physical Review Letters*, 81, 1562  
 Gunn J. E., et al., 2006, *AJ*, 131, 2332  
 Guzik J., Bernstein G., Smith R. E., 2007, *MNRAS*, 375, 1329  
 Hamann J., Hannestad S., Melchiorri A., Wong Y. Y. Y., 2008, *J. Cosmology Astropart. Phys.*, 7, 17  
 Hannestad S., 2003, *Phys. Rev. D*, 67, 085017  
 Hannestad S., 2005, *Physical Review Letters*, 95, 221301  
 Hannestad S., 2010, preprint (arXiv:1007.0658)  
 Hannestad S., Tu H., Wong Y. Y., 2006, *J. Cosmology Astropart. Phys.*, 6, 25  
 Hannestad S., Wong Y. Y. Y., 2007, *J. Cosmology Astropart. Phys.*, 7, 4  
 Hauser M. G., Peebles P. J. E., 1973, *ApJ*, 185, 757  
 Heavens A. F., Matarrese S., Verde L., 1998, *MNRAS*, 301, 797  
 Ichikawa K., Fukugita M., Kawasaki M., 2005, *Phys. Rev. D*, 71, 043001  
 Ichiki K., Takada M., Takahashi T., 2009, *Phys. Rev. D*, 79, 023520  
 Jain B., Bertschinger E., 1994, *ApJ*, 431, 495  
 Jeong D., Komatsu E., 2009, *ApJ*, 691, 569  
 Jimenez R., Kitching T., Peña-Garay C., Verde L., 2010, *J. Cosmology Astropart. Phys.*, 5, 35  
 Juszkiewicz R., 1981, *MNRAS*, 197, 931  
 Kass R. E., Raftery A. E., 1995, *Journal of the American Statistical Association*, 90, 773  
 Kiakotou A., Elgarøy Ø., Lahav O., 2008, *Phys. Rev. D*, 77, 063005  
 Komatsu E., et al., 2010, preprint (arXiv:1001.4538)  
 Lahav O., Kiakotou A., Abdalla F. B., Blake C., 2010, *MNRAS*, 405, 168  
 Lesgourgues J., Matarrese S., Pietroni M., Riotto A., 2009, *J. Cosmology Astropart. Phys.*, 6, 17  
 Lesgourgues J., Pastor S., 2006, *Phys. Rep.*, 429, 307  
 Lesgourgues J., Pastor S., Perotto L., 2004, *Phys. Rev. D*, 70, 045016  
 Lewis A., Bridle S., 2002, *Phys. Rev. D*, 66, 103511  
 Li C., Kauffmann G., Jing Y. P., White S. D. M., Börner G., Cheng F. Z., 2006, *MNRAS*, 368, 21  
 Makino N., Sasaki M., Suto Y., 1992, *Phys. Rev. D*, 46, 585  
 Mantz A., Allen S. W., Rapetti D., 2010, *MNRAS*, 406, 1805  
 Marshall P., Rajguru N., Slosar A., 2006, *Phys. Rev. D*, 73, 067302  
 Martin R., 2009, preprint (arXiv:0905.4907)  
 McDonald P., 2006, *Phys. Rev. D*, 74, 103512  
 Morgan J. S., Burgett W., Teran J. U., 2008, in Stepp L. M., Gilmozzi R., eds, *Proc. SPIE Vol. 7012, Ground-based and Airborne Telescopes II*. SPIE, Bellingham, p. 70122R  
 Morgan J. S., Kaiser N., 2008, in Stepp L. M., Gilmozzi R., eds, *Proc. SPIE Vol. 7012, Ground-based and Airborne Telescopes II*. SPIE, Bellingham, p. 70121K  
 Norberg P., et al., 2001, *MNRAS*, 328, 64  
 Norberg P., et al., 2002, *MNRAS*, 332, 827  
 Park C., Vogeley M. S., Geller M. J., Huchra J. P., 1994, *ApJ*, 431, 569  
 Peacock J. A., Dodds S. J., 1994, *MNRAS*, 267, 1020  
 Peebles P. J. E., 1980, *The Large-Scale Structure of the Universe*. Princeton Univ. Press, Princeton, NJ  
 Percival W. J., et al., 2001, *MNRAS*, 327, 1297  
 Percival W. J., et al., 2010, *MNRAS*, 401, 2148  
 Percival W. J., et al., 2007, *ApJ*, 657, 645  
 Percival W. J., Verde L., Peacock J. A., 2004, *MNRAS*, 347, 645  
 Reid B. A., Verde L., Jimenez R., Mena O., 2010a, *J. Cosmology Astropart. Phys.*, 1, 3  
 Reid B. A., et al., 2010b, *MNRAS*, 404, 60  
 Saito S., Takada M., Taruya A., 2008, *Physical Review Letters*, 100, 191301  
 Saito S., Takada M., Taruya A., 2009, *Phys. Rev. D*, 80, 083528

- Saito S., Takada M., Taruya A., 2010, preprint (arXiv:1006.4845)
- Sánchez A. G., Cole S., 2008, MNRAS, 385, 830
- Schulz A. E., White M., 2006, Astroparticle Physics, 25, 172
- Scoccimarro R., 2004, Phys. Rev. D, 70, 083007
- Scoccimarro R., Frieman J., 1996, ApJS, 105, 37
- Seaborne M. D., et al., 1999, MNRAS, 309, 89
- Seljak U., 2000, MNRAS, 318, 203
- Seljak U., 2001, MNRAS, 325, 1359
- Sheth R. K., Lemson G., 1999, MNRAS, 304, 767
- Smith J. A., et al., 2002, AJ, 123, 2121
- Smith R. E., et al., 2003, MNRAS, 341, 1311
- Strauss M. A., et al., 2002, AJ, 124, 1810
- Sunyaev R. A., Zeldovich Y. B., 1970, Ap&SS, 7, 3
- Swanson M. E. C., Tegmark M., Blanton M., Zehavi I., 2008, MNRAS, 385, 1635
- Takada M., Komatsu E., Futamase T., 2006, Phys. Rev. D, 73, 083520
- Taruya A., Nishimichi T., Saito S., Hiramatsu T., 2009, Phys. Rev. D, 80, 123503
- Tegmark M., et al., 2004, Phys. Rev. D, 69, 103501
- Tegmark M., et al., 2006, Phys. Rev. D, 74, 123507
- Tereno I., Schimd C., Uzan J., Kilbinger M., Vincent F. H., Fu L., 2009, A&A, 500, 657
- Thomas S. A., Abdalla F. B., Lahav O., 2010, Physical Review Letters, 105, 031301
- Vikhlinin A., et al., 2009, ApJ, 692, 1060
- Wake D. A., et al., 2008, MNRAS, 387, 1045
- Wendell R., et al., 2010, Phys. Rev. D, 81, 092004
- Wild V., et al., 2005, MNRAS, 356, 247
- Wong Y. Y. Y., 2008, J. Cosmology Astropart. Phys., 10, 35
- Zehavi I., et al., 2005, ApJ, 621, 22
- Zehavi I., et al., 2002, ApJ, 571, 172